

## **PROJECT 2.1: OBSERVED AND MODELLED CLIMATE FOR THE NORTH-WEST**

### **Principal Investigator**

*Leon D. Rotstayn*, CSIRO Marine and Atmospheric Research, Aspendale, Vic 3195, Australia and The Centre for Australian Weather and Climate Research, a partnership between CSIRO and the Bureau of Meteorology,  
Ph: 03 9239 4542; Email: [Leon.Rotstayn@csiro.au](mailto:Leon.Rotstayn@csiro.au)

### **Objectives**

- To refine the high-resolution CSIRO climate model (Mk3.5A) so that it achieves a stable, high-resolution simulation of present global climate, including aerosols, and an evaluation of this simulation. (The inclusion of aerosols is non-trivial task.)
- To describe the observed climate changes, the modelled changes and their limitations; and then incorporate *time-varying* aerosol forcing into model with the aim of capturing the observed rainfall increases with increased confidence.
- To investigate the effects of aerosols and greenhouse gases on past and future rainfall trends in the North-West using the Mk3.5A model.
- To ascertain the prognosis associated with reduction in air-pollution over the next few decades.

### **Key Research Findings**

- A new version of CSIRO's high resolution global climate model (Mk3.6 GCM) has been constructed. Mk3.6 includes a comprehensive, interactive aerosols scheme. This model will be used to further investigate the extent to which the observed rainfall increase in the North-West is being driven by the Asian aerosol haze.
- Comparison of the mean summer and winter climate simulations in Mk3.6 with those of its predecessors show several encouraging improvements in the

new version, especially with regard winter rainfall and mean sea level pressure (MSLP). The improved simulation of winter rainfall over south-western WA makes the Mk3.6 model potentially attractive for use in downscaling studies over that region.

- The predecessors of Mk3.6 (Mk3.5 and Mk3.0) have been previously ranked as 12<sup>th</sup> and equal 13<sup>th</sup> out of the 23 GCMs used in the IPCC AR4. Using the same assessment criterion, the improved performance of Mk3.6 would rank it fifth out of 24 GCMs.
- In comparison with its predecessors, the most dramatic improvement in Mk3.6 was in the model's simulation of the leading modes of annual rainfall variability. Mk3.6 was best able to capture the spatial pattern of the leading El Niño Southern Oscillation (ENSO) related rainfall mode, which is centred over eastern Australia, whereas earlier versions incorrectly located the centre of this mode over WA. This improvement is important, because if the ENSO-related mode in the model is located over northern WA, the simulated rainfall response there may be unrealistically dominated by the response of ENSO to the applied forcing.
- In comparison with seven other GCMs, Mk3.6 has the best simulation of the spatial pattern of the two leading modes of Australian rainfall variability. The second rainfall mode, centred over north-western WA, was also captured best by Mk3.6, although the correlation of this mode with ENSO was too strong.
- An accurate simulation of the first rainfall mode is important for studies of Australian climate change, because this mode correlates strongly with ENSO, which dominates rainfall variability over most of eastern and central Australia. The second rainfall mode is also potentially important, because its observed time series shows a significant upward trend in recent decades, corresponding to increased rainfall over northern WA, and decreased rainfall over eastern Australia.

**MILESTONE 2.1.1: IS THE HIGH-RESOLUTION SIMULATION OF PRESENT CLIMATE INCLUDING AEROSOLS COMPARABLE TO OR BETTER THAN THE EARLIER VERSION WITHOUT AEROSOLS?**

**Background**

We assess the simulation of Australian mean climate and rainfall variability in a new version of the CSIRO global climate model (GCM). The new version, called Mark 3.6 (Mk3.6) differs most substantially from its recent predecessors (Mk3.0 and Mk3.5) by inclusion of a comprehensive aerosol scheme, which treats a range of climatically important aerosols (atmospheric particles). Comparison of the mean summer and winter climate simulations in Mk3.6 with those in Mk3.0 and Mk3.5 shows several improvements in the new version, especially regarding winter rainfall and sea-level pressure. Over Western Australia (WA), the simulation of winter rainfall is much improved relative to the earlier versions of the model: Although Mk3.6 is somewhat too dry over southwest Western Australia (SWWA), it does not exhibit the severe dryness of Mk3.5 or the unrealistic winter rainfall over the north-west that was seen in Mk3.0. The improved simulation of winter rainfall over the south-west makes the Mk3.6 GCM potentially attractive for use in downscaling studies over that region.

The conclusion that Mk3.6 provides an improved overall simulation of Australian mean climate is further supported by calculation of Watterson's non-dimensional M-statistic, using observations of rainfall, surface air temperature and sea-level pressure for all four seasons.  $M = 0$  indicates no skill, and  $M = 1$  indicates perfect skill. Using observations for 1958 – 2001, as in Watterson (2008), the Mk3.6 simulation achieved  $M = 0.655$ , compared to 0.607 for Mk3.5 and 0.601 for Mk3.0. The best-ranked model (ECHAM5 from the Max Planck Institute for Meteorology) achieved  $M = 0.700$ , while the worst-ranked model scored  $M = 0.304$ . Including Mk3.6 in Table 1 of Watterson (2008) would make it fifth out of 24 models.

However, the most dramatic improvement occurs in the model's simulation of the leading mode of annual rainfall variability, which we assess using empirical

orthogonal teleconnections (EOTs). Mk3.6 is best able to capture the spatial pattern of the leading rainfall mode, which is centred over eastern Australia, whereas the earlier versions incorrectly locate the centre of this mode over northern WA. This mode correlates strongly with the El Niño Southern Oscillation (ENSO), which dominates rainfall variability over much of Australia, so its accurate simulation is crucial for studies of Australian climate change. This improvement is important, because if the ENSO-related mode in the model is incorrectly located over northern WA, the simulated rainfall response there may be unrealistically dominated by the response of ENSO to the applied forcing.

The EOT analysis is repeated using output from five international GCMs, which were recently assessed as providing a good simulation of Australian mean seasonal climate. Of the models considered, Mk3.6 has the best simulation of the spatial pattern and properties of the leading mode of Australian rainfall variability.

The second rainfall mode, centred over northern WA, is also captured best by Mk3.6, although the correlation of this mode with ENSO is too strong. The overly strong correlation with ENSO is probably related to an excessive westward extension of the ENSO-related sea-surface temperature anomalies, a typical GCM bias that was seen in all the models we looked at. The second rainfall mode is potentially important, because its observed time series shows a significant upward trend in recent decades, corresponding to increased rainfall in the north-west, and decreased rainfall over eastern Australia. With regard to the aims of this project, it is encouraging that the Mk3.6 GCM is able to capture this pattern as an unforced mode of natural variability (though its physical meaning is currently unexplained). It will be most interesting to see whether this mode responds differently in time-varying simulations that include changes in Asian aerosol forcing, as hypothesized by Rotstayn *et al.* (2007).

Observations show increased rainfall in north-western Australia in recent decades but climate simulations forced by increasing greenhouse gases have generally not reproduced this trend. An exploratory study with a low-resolution version of the CSIRO climate model suggests that a possible cause of the rainfall increase is the massive Asian haze, which consists mainly of fine particles (aerosols) of human origin (Rotstayn *et al.*, 2007). The haze cools the Asian continent and nearby oceans,

thus changing the delicate balance of temperature and monsoonal winds between Asia and Australia. There are large uncertainties in this recent study, including the coarse resolution of the model, which means that modes of variability affecting Australian rainfall, such as El Niño Southern Oscillation (ENSO), are not well simulated.

### *Objectives*

To refine the high-resolution CSIRO climate model (Mk3.6) so that it achieves a stable, high-resolution simulation of present global climate, including aerosols, and to provide an evaluation of this simulation.

Australia faces serious challenges due to rainfall deficits over much of the east and southwest of the country. In public discourse, it is common for these rainfall deficits to be attributed to the enhanced greenhouse effect, but in reality the situation is far more complex.

Australian rainfall variability is modulated by natural oscillations in the ocean basins to the east, south, and west of Australia. The influence of ENSO has been known for many years, with El Niño events associated with low rainfall over the eastern two-thirds of Australia, especially during austral spring (McBride and Nicholls, 1983; Ropelewski and Halpert, 1987). To the west, recent research has focused on a natural mode referred to as the Indian Ocean Dipole (Saji *et al.*, 1999) and its link to Australian wintertime rainfall variations in a broad band stretching from the northwest to the southeast of the continent (Ashok *et al.*, 2003). To the south, the Southern Annular Mode (SAM) is the major mode of variability. It has been linked to interannual rainfall variations over southern Australia, both in the southwest (Cai *et al.*, 2003b) and the southeast (Meneghini *et al.*, 2007). At least in part, the response of Australian rainfall changes to anthropogenic forcing is likely to involve the interaction of the forcing with these natural modes of variability (e.g., Shi *et al.*, 2008b).

Modelling suggests that the recent trend in the SAM is due, at least in part, to Antarctic ozone depletion and increasing greenhouse gases (e.g., Arblaster and Meehl,

2006). Because the SAM has been linked to rainfall variations in the southwest, this suggests that these forcings have an important role in the rainfall decline there. However, there are still ambiguities in making this connection (Timbal *et al.*, 2006). Recent climate modelling suggests that anthropogenic aerosols from the Northern Hemisphere may have also contributed to the trend in the SAM, and by implication, to the decline in rainfall in the southwest (Cai and Cowan, 2007). Other studies have suggested land-cover change (Pitman *et al.*, 2004; Timbal and Arblaster, 2005 ) or natural multi-decadal fluctuations (Cai *et al.*, 2005) as possible causes of the rainfall decline in the southwest.

Meanwhile, the northwest and central parts of Australia have experienced increased rainfall in recent decades, which has prompted calls to shift agriculture from the increasingly dry south to the north. However, recent climate modelling suggests that the rainfall increase in the northwest may be driven by the Asian aerosol haze, rather than increasing greenhouse gases (Rotstayn *et al.*, 2007). This raises the possibility that the recent rainfall increase in the northwest may be a transitory phenomenon, and that a major decision to move agricultural infrastructure could be based on an overly simplistic view of climate-change science (Flannery, 2007).

For policymakers and researchers working on climate impacts and adaptation, very different rainfall futures are implied by different drivers of recent rainfall changes. A rainfall change attributed to natural variability will be a passing phenomenon, and changes related to ozone depletion or anthropogenic aerosols are likely to be more transitory than changes related to increasing greenhouse gases.

This situation suggests an urgent need for a high-quality climate-modelling capacity in Australia, so that the key drivers of recent rainfall trends can be better understood. With a long-term view, the Australian climate-science community has begun the development of a new modelling system (ACCESS – the Australian Community Climate and Earth System Simulator; Smith, 2007). However, it is likely to be some years before this new system has been fully developed and tested to provide a robust modelling platform. An existing Australian climate model, developed at the Commonwealth Scientific and Industrial Research Organisation (CSIRO) since the early 1980s, was included in the Fourth Assessment Report (AR4) of the

Intergovernmental Panel on Climate Change (IPCC), and can potentially be used to fill the gap during the next few years.

The above findings regarding possible aerosol effects on north-western Australian rainfall (Rotstayn *et al.*, 2007) and the SAM (Cai and Cowan, 2007) suggest that a climate model used for the study of Western Australian regional climate change needs to include a comprehensive aerosol treatment. However, the low-resolution version of the CSIRO global climate model (GCM) referred to above has certain deficiencies that limit its usefulness in the study of regional climate change, such as a poor simulation of ENSO and ENSO-related rainfall variability (Rotstayn *et al.*, 2007; Shi *et al.*, 2008a). For this reason, the aerosol treatments used by Rotstayn *et al.* (2007) were ported to the high-resolution Mk3.5 coupled atmosphere-ocean GCM, one of two model versions submitted by CSIRO to AR4.

Recent studies suggest that Mk3.0 and Mk3.5 are roughly mid-ranking models in their simulation of Australian mean seasonal climate. A detailed assessment of the mean seasonal Australian climate simulations of 23 AR4 GCMs was carried out by Suppiah *et al.* (2007). Based on their scoring system, the CSIRO Mk3.0 GCM was ranked equal 12<sup>th</sup> out of 23 models. (Mk3.5 was not included in this study, as it was submitted too late to AR4.) Watterson (2008) used the “M-statistic” (Watterson, 1996; Meehl *et al.* 2007) to provide a non-dimensional skill score for the simulation of Australian mean seasonal climate in 23 AR4 GCMs. Mk3.0 and Mk3.5 were respectively ranked equal 13<sup>th</sup> and 12<sup>th</sup> out of 23 models.

Before embarking on studies of climate change or variability with a new model, it is essential to evaluate the performance of the model, since inclusion of ostensible improvements can easily degrade the climatology of a model, which will normally have been optimised around existing model treatments. The motivation for the first phase of Project 2.1 was to assess the simulation of Australian and Western Australian climate in a new version of the model, Mk3.6 (previously called Mk3.5A). An important focus of this report is the simulation of natural rainfall variability. To adequately capture rainfall variability, a model must simulate realistic sea-surface temperature (SST) anomalies and the associated atmospheric teleconnections – an assessment far more demanding than mean rainfall alone. We find the simulation of

rainfall variability to be more realistic in Mk3.6 than in the standard Mk3.5 model. In Section 3, the models and data are described. In Section 4, the Mk3.6 model's simulation of mean Australian seasonal climate is compared with observations and other versions of the model. In Section 5, we assess key modes of Australian rainfall variability, such as those associated with ENSO, in the model and in several AR4 models. Section 6 contains a summary.

## **Technical Details**

### Models and data

The CSIRO Mk3.0 GCM is described in detail by Gordon *et al.* (2002). The Mk3.5 version included a number of changes with a view to reducing errors in Mk3.0; these are summarized by Rotstayn *et al.* (2009). The main difference between Mk3.5 and Mk3.6 is the incorporation of an interactive aerosol scheme in Mk3.6. The aerosol species treated by the model are sulfate, carbonaceous aerosol, mineral dust and sea salt. "Interactive" means that the model's meteorology affects the aerosol distribution, and the aerosols can alter the meteorology via their direct and indirect effects on radiation. (Indirect effects occur when aerosols modify the properties of clouds.) Other differences between Mk3.5 and Mk3.6 are the inclusion of an updated radiation scheme, improvements to the boundary-layer mixing scheme and changes to the treatment of convective cloud. The Mk3.6 model is described in detail by Rotstayn *et al.* (2009).

In the next two sections, we show results from a 70-year control simulation of the Mk3.6 coupled atmosphere-ocean model, with forcing (greenhouse gases, aerosols and ozone) prescribed for the year 2000. This run was initialised from a 260-year "spin-up" run of the Mk3.6 model, which was designed to allow the model to equilibrate to the inclusion of the new aerosol treatments. The 70-year control run is compared with output from 20<sup>th</sup> Century transient simulations (with time-varying forcing) of the Mk3.0 and Mk3.5 models and from several other AR4 models. In effect, we assume that the 70-year coupled run with fixed forcing for the year 2000 provides a reasonable proxy for late 20<sup>th</sup> Century climate. This approximation was necessary because we currently have no 20<sup>th</sup> Century transient simulation with Mk3.6,

and (given current computational resources) it will be some time before we have such a simulation. The generally favourable results obtained with Mk3.6 suggest that the use of this approximation is not a serious problem.

We use observations of sea-level pressure from HadSLP2 (Allan and Ansell, 2006), and rainfall and surface air temperature from the Australian Bureau of Meteorology (Jones and Weymouth, 1997; Jones and Trewin, 2000). SST observations are from HadISST (Rayner *et al.*, 2003).

**Table 2.1.1: AR4 models used in this study, with their ranking (out of 23 models) for simulation of Australian mean seasonal climate from Suppiah *et al.* (2007) and Watterson (2008).**

Model	Origin	Ranking (Suppiah)	Ranking (Watterson)
CSIRO-Mk3.0	CSIRO Atmospheric Research, Australia	= 12	= 13
CSIRO-Mk3.5	CSIRO Marine and Atmospheric Res., Australia	N/A	12
ECHAM5	Max Planck Institute, Germany	1	1
GFDL-CM2.1	Geophysical Fluid Dynamics Laboratory, USA	= 2	4
HadGEM1	Hadley Centre, United Kingdom	= 2	3
MIROC3.2 (med)	Centre for Climate Research, Japan	= 12	9
MRI-CGCM2.3.2	Meteorological Research Institute, Japan	6	= 13

Our assessment of rainfall variability (in section 5) includes the CSIRO Mk3.6 GCM and seven AR4 GCMs (including Mk3.0 and Mk3.5). The non-CSIRO AR4 models include ECHAM5, the model that received the highest ranking for simulation of Australian mean seasonal climate by Suppiah *et al.* (2007) and Watterson (2008), and two other models that were ranked narrowly behind ECHAM5 in both studies (GFDL CM2.1 and HadGEM1). The AR4 models are listed in Table 2.1.1, together with their rankings from Suppiah *et al.* (2007) and Watterson (2008). We include MIROC3.2

(medium resolution) in our analysis, because (in common with Mk3.6) it includes direct and indirect aerosol effects in an interactive scheme, which treats sulfate, carbonaceous aerosol, mineral dust and sea salt (Takemura *et al.*, 2000). Note that the aerosol treatments in many other AR4 models were not interactive. For example, GISS-ER includes the aerosol effects referred to above, but used prescribed time-varying aerosol fields. Further details of the AR4 models are available at [http://www-pcmdi.llnl.gov/ipcc/model\\_documentation/ipcc\\_model\\_documentation.php](http://www-pcmdi.llnl.gov/ipcc/model_documentation/ipcc_model_documentation.php).

#### *Mean summer and winter climate simulations*

In this section, we present a basic assessment of the Australian winter and summer climate simulations of Mk3.0, Mk3.5 and Mk3.6. Observations, and model output from Mk3.0 and Mk3.5, are for the period 1981-1999. In addition to visual assessment of the modelled and observed fields, we calculate pattern correlations and root-mean-square (RMS) errors. (Pattern correlations measure the similarity between the *pattern* of observed and modelled values, with a value of 1 denoting perfect agreement. However, pattern correlations are not sensitive to the *magnitude* of the differences. For this reason, they are supplemented by RMS errors, which provide a measure of the magnitude of the errors in the modelled fields.) Prior to these calculations, all data were interpolated to the 0.5° by 0.5° grid on which the observations from the Bureau of Meteorology were provided.

Figures 2.1.1 and 2.1.2 show observed and modelled surface air temperature for the winter (JJA) and summer (DJF) seasons respectively. Mk3.0 tends to have a cool bias (especially in winter), Mk3.5 tends to have a warm bias (especially in summer), and Mk3.6 falls between the other two. The models as a group tend to be cooler (relative to the observations) in winter than in summer. For example, Mk3.5 does not have a warm bias over all parts of the continent in winter, when it actually has a cool bias over southern Australia. Table 2.2.2 shows little difference in the pattern correlations between the models, since all three versions are broadly able to capture the strong north-south temperature gradient over the continent. The RMS errors show that Mk3.5 has the smallest cool bias in winter, and Mk3.0 the largest. In summer, the warm bias in Mk3.5 is consistent with its relatively large RMS error, and Mk3.6 has the lowest RMS error of the three. In summary, the RMS errors for surface air

temperature suggest that Mk3.0 is least realistic, Mk3.5 is best in winter, and Mk3.6 is best in summer.

**Table 2.2.2: Model – observed pattern correlations and RMS errors (°C) for surface air temperature over Australia**

	Mk3.0		Mk3.5		Mk3.6	
	correlation	RMS	correlation	RMS	correlation	RMS
JJA	0.93	3.6	0.95	1.6	0.95	2.7
DJF	0.95	1.6	0.96	2.7	0.94	1.3

Mean sea-level pressure (MSLP) is shown in Figures 2.1.3 and 2.1.4, for JJA and DJF respectively. In JJA, Mk3.0 and Mk3.5 have a high bias in MSLP across subtropical latitudes, and this is not seen in Mk3.6. Also, the overly zonal (east-west) pattern south of Australia in Mk3.5 is much improved in Mk3.6. This is encouraging, as it suggests that Mk3.6 will be more successful at capturing the synoptic systems that bring rainfall to southern Australia. However, in DJF, the excessively deep low-pressure centre over north-western Australia is worse in Mk3.6 than in the earlier versions. In Table 2.1.3, the relatively poor JJA MSLP simulation in Mk3.5 and the improved simulation in Mk3.6 are clearly seen in the RMS errors. In DJF, the effect of the overly deep “heat low” over the northwest in Mk3.6 is also reflected in its larger RMS error. The pattern correlations show that all three models are generally able to capture the spatial pattern of MSLP in JJA and DJF, though in JJA there is some improvement in the sequence Mk3.0 – Mk3.5 – Mk3.6.

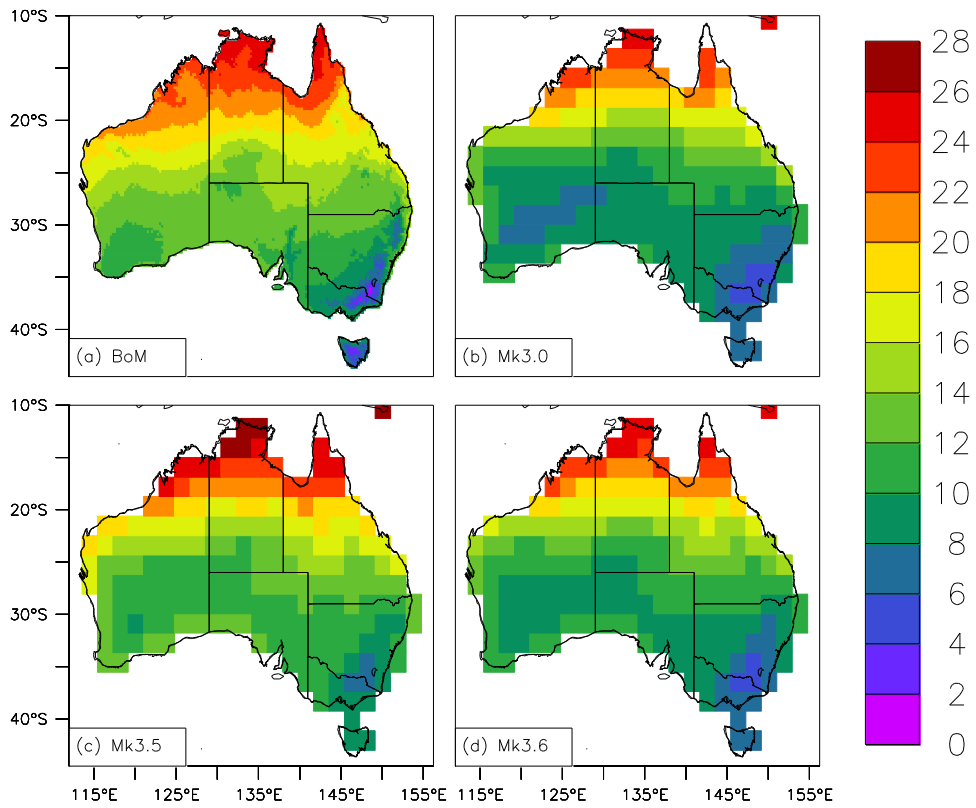


**Figure 2.1.1: JJA surface air temperature in °C, (a) from observations for the period 1981-1999, and simulated by three versions of the CSIRO GCM: (b) Mk3.0, (c) Mk3.5 and (d) Mk3.6.**

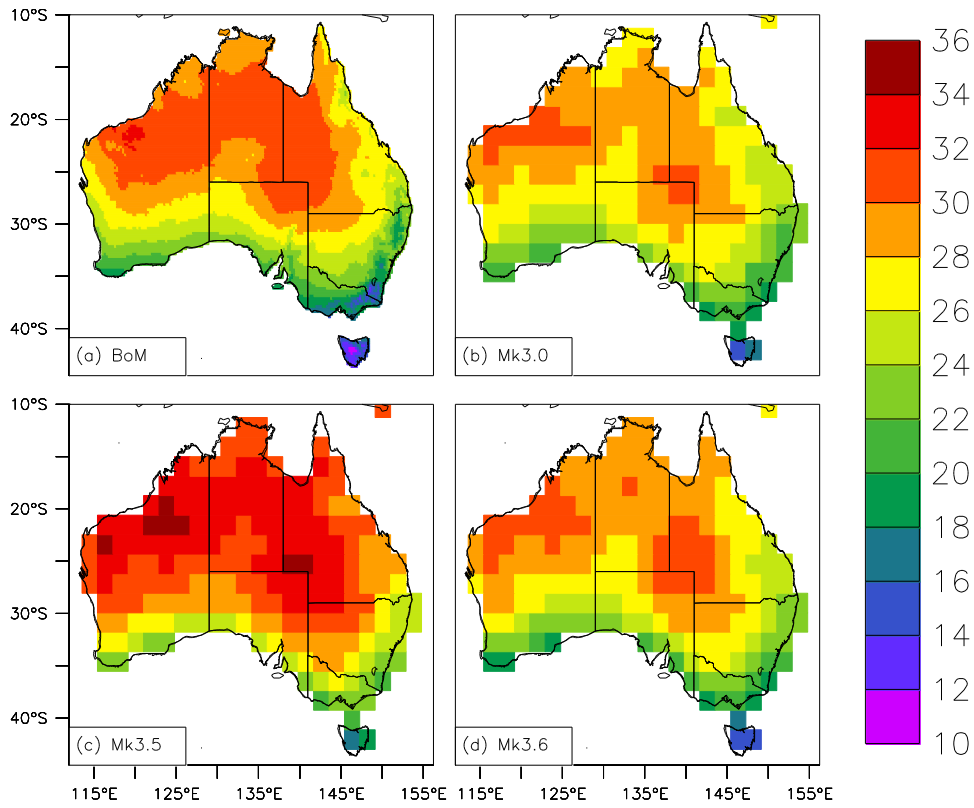


**Figure 2.1.2: DJF surface air temperature in °C, (a) from observations for the period 1981-1999, and simulated by three versions of the CSIRO GCM: (b) Mk3.0, (c) Mk3.5 and (d) Mk3.6.**

**Table 2.1.3: Model – observed pattern correlations and RMS errors (hPa) for MSLP over Australia**

	Mk3.0		Mk3.5		Mk3.6	
	correlation	RMS	correlation	RMS	correlation	RMS
JJA	0.90	1.4	0.93	2.5	0.96	0.8
DJF	0.95	1.4	0.96	1.4	0.96	3.1

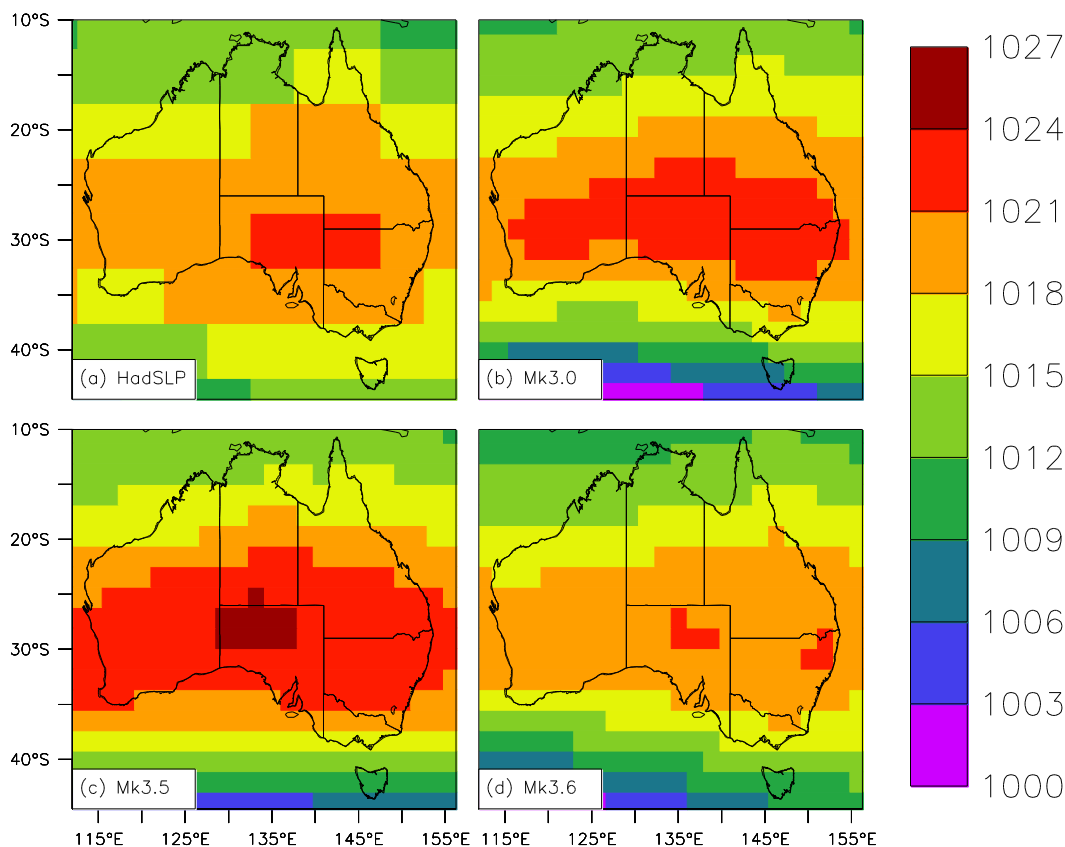


**Figure 2.1.3: JJA mean sea-level pressure in hPa, (a) from observations for the period 1981-1999, and simulated by three versions of the CSIRO GCM: (b) Mk3.0, (c) Mk3.5 and (d) Mk3.6.**

Precipitation is a challenging field for climate models to simulate well, but is critical for this project. Figures 2.1.5 and 2.1.6 show observed and modelled precipitation, for JJA and DJF respectively. In JJA, Mk3.0 has a good simulation over southern Australia, but is affected by an unrealistic pattern over north-western and central Australia. Mk3.5 is much too dry over southern Australia; this is a serious problem if the modelled rainfall in a region is so low that it makes it difficult to plausibly study changes in rainfall under perturbed forcing. Mk3.6 looks like an improved version of Mk3.5: It is still too dry in the south, but the bias is reduced, especially over Victoria and the south-western corner of Western Australia (WA). In DJF, all versions of the model do a reasonable job of capturing the observed precipitation pattern, albeit with too much penetration of rainfall into the dry south-west. Mk3.6 produces excessive rainfall over the wettest areas in the tropics, seen at a few grid points in the far north in Figure 2.1.6; this is probably related to the revision of the convective cloud treatment, rather than anything related to interactive aerosols (Rotstajn *et al.*, 2009).

Referring to Table 2.1.4, Mk3.6 achieves clearly the best precipitation simulation in JJA, with the highest pattern correlation and the lowest RMS error. In DJF, the effect of the excessive tropical rainfall in Mk3.6 is seen in its relatively large RMS error, although it still has a slightly better pattern correlation than the other two versions.

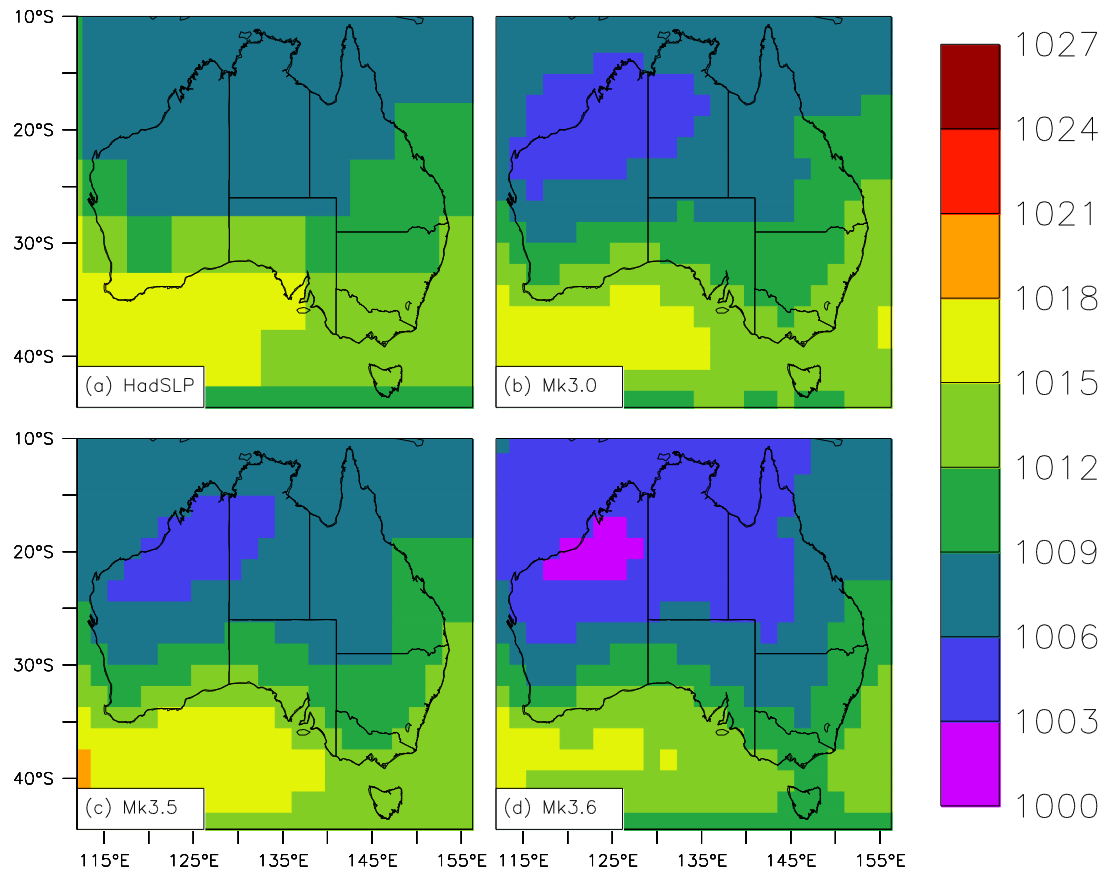


**Figure 2.1.4: DJF mean sea-level pressure in hPa, (a) from observations for the period 1981-1999, and simulated by three versions of the CSIRO GCM: (b) Mk3.0, (c) Mk3.5 and (d) Mk3.6.**

**Table 2.1.4: Model – observed pattern correlations and RMS errors (mm/day) for precipitation over Australia**

	Mk3.0		Mk3.5		Mk3.6	
	correlation	RMS	correlation	RMS	correlation	RMS
JJA	0.61	0.65	0.74	0.66	0.86	0.51
DJF	0.90	1.3	0.89	1.0	0.92	1.7

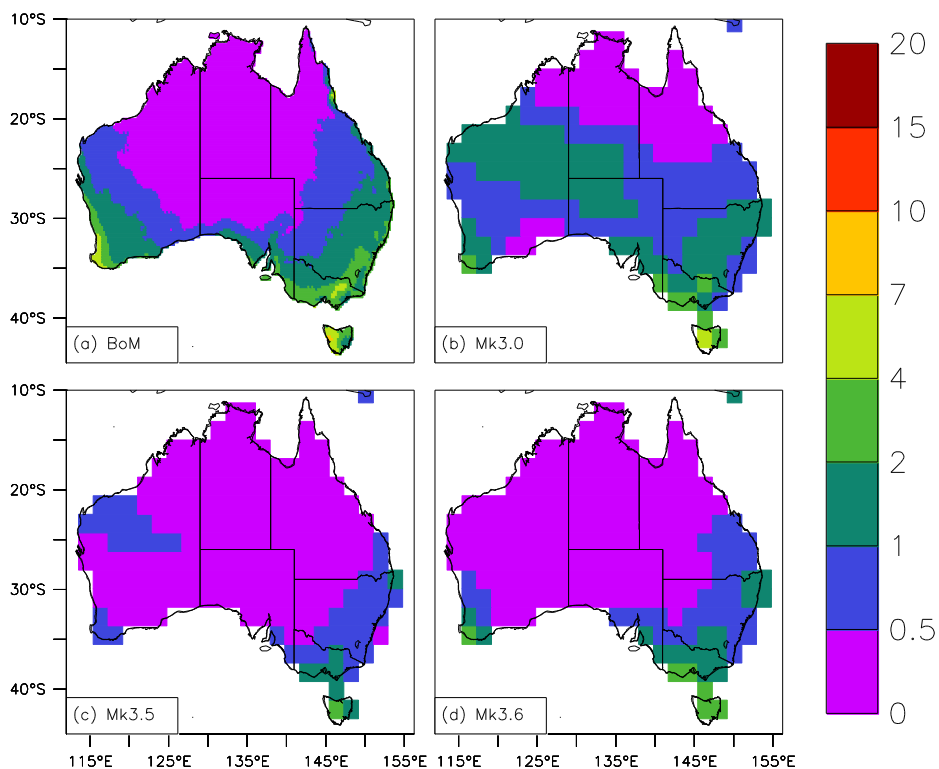


**Figure 2.1.5: JJA precipitation in mm/day, (a) from observations for the period 1981-1999, and simulated by three versions of the CSIRO GCM: (b) Mk3.0, (c) Mk3.5 and (d) Mk3.6.**

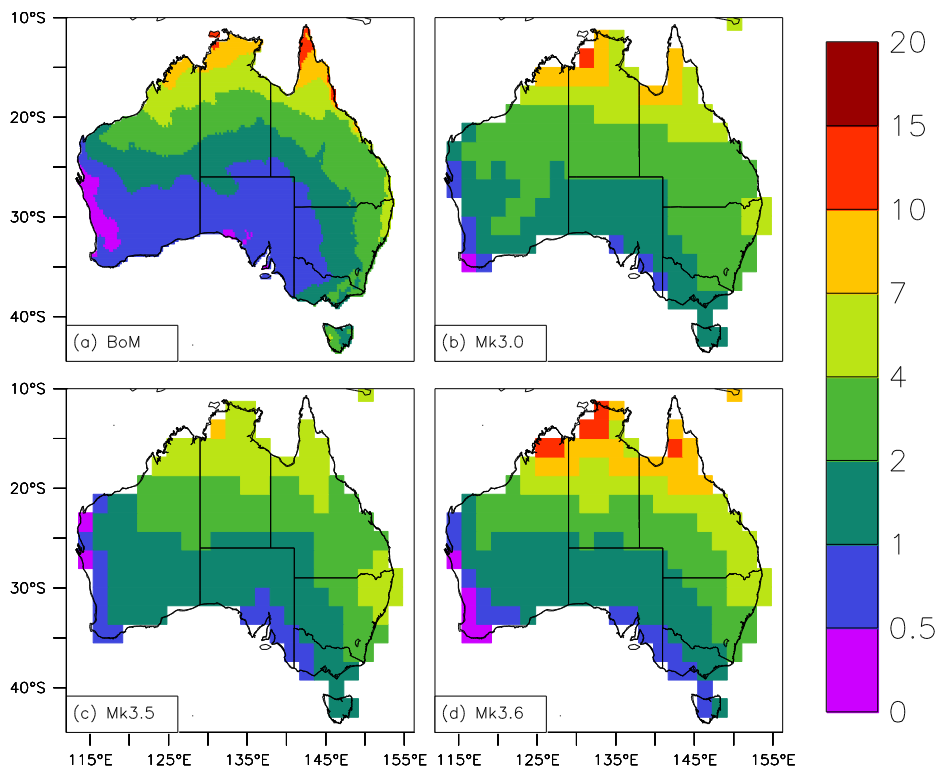


**Figure 2.1.6: DJF precipitation in mm/day, (a) from observations for the period 1981-1999, and simulated by three versions of the CSIRO GCM: (b) Mk3.0, (c) Mk3.5 and (d) Mk3.6.**

Based on its simulation of mean summer and winter climate over Australia, the Mk3.6 model shows some encouraging improvements relative to the earlier versions of Mk3, although the improvement is not uniform. Some of the biases identified over Australia are simply regional versions of biases that are seen more globally in that model version. For example, Mk3.5 tends to have a warm bias on global scales, and Mk3.6 generates excessive convection elsewhere in the tropics. It is possible that radiative heating due to mineral dust has exacerbated a pre-existing tendency for the model to generate an overly deep heat low over northwest Australia in summer (cf. Mohalfi *et al.*, 1998). Of the three model versions, Mk3.6 provides arguably the best simulation of Australian summer and winter mean climate. The temperature simulation achieves a better compromise than the other two versions, and the winter MSLP simulation is much improved. The winter rainfall pattern, while somewhat too dry in the south, does not exhibit the severe dryness of Mk3.5 or the unrealistic winter rainfall over the north-west and centre that was seen in Mk3.0. Over WA, the simulation of winter rainfall is much improved relative to the earlier versions of the model.

The conclusion that Mk3.6 provides an improved simulation of Australian mean climate is further supported by calculation of the non-dimensional M-statistic (Watterson, 1996; Meehl *et al.*, 2007), using observations of rainfall, surface air temperature and MSLP for all four seasons.  $M = 0$  indicates no skill, and  $M = 1$  indicates perfect skill. Using observations for 1958 – 2001, as in Watterson (2008), the Mk3.6 simulation achieved  $M = 0.655$ , compared to 0.607 for Mk3.5 and 0.601 for Mk3.0. The best-ranked model (ECHAM5) achieved  $M = 0.700$ , while the worst-ranked model scored  $M = 0.304$ . Including Mk3.6 in Table 2.1.1 of Watterson (2008) would make it fifth out of 24 models.

### *Modes of Australian rainfall variability and ENSO*

A crucial test of a model intended for the study of Australian climate change is its ability to simulate the variability of Australian rainfall. As was discussed in the Introduction, Australian rainfall variability is associated with natural oscillations in the surrounding ocean basins. In this section we assess the simulation of Australian rainfall variability in the Mk3.6 GCM along with several other models. We also

briefly consider how the models' simulation of Australian rainfall variability relates to their simulation of ENSO.

Empirical orthogonal teleconnections (EOTs; van den Dool *et al.*, 2000) are a useful tool for analysis of rainfall patterns. Smith (2004) used EOT analysis in a study of Australian rainfall trends, and argued that EOTs are better suited for analysis of rainfall data than empirical orthogonal functions (EOFs). EOFs are based on a calculation of global variance, namely, the sum of the anomalies squared over the area of interest. This is not necessarily desirable for rainfall, because squaring the anomalies creates a strong bias towards the areas with the largest totals (typically, the Tropics). A more natural approach is to use the global integral as a descriptor (in this case, the all-Australian rainfall). The method, which is simpler than the calculation of EOFs, is outlined in the next paragraph (with more details in Smith, 2004).

The first step is to find the grid point whose time series (T1) most closely matches the all-Australian annual-mean rainfall time series. The second step is to perform a linear regression of T1 with the rainfall time series at each grid point, and generate a map of correlation coefficients. This map (with  $r = +1$  centred on the chosen grid point) is the first spatial mode or teleconnection pattern (EOT1). If raw (non-detrended) rainfall observations for 1901–2007 are used, the result is as shown in Figure 2.1.7a. This first mode could be described as a “central-east” mode, and describes 62% of the variance. It could also be described as an “ENSO-like” mode, because it resembles the pattern obtained when Australian annual rainfall is regressed against the Southern Oscillation Index (SOI), and it has a strong positive correlation with the SOI and a strong negative correlation with SST averaged over the Niño 3.4 region in the tropical eastern Pacific (170°W–120°W, 5°S–5°N). The next step in the analysis is to subtract the result of the above linear regression from the data at each grid point, thereby removing the influence of the first mode. The all-Australian rainfall is re-calculated using the remaining data, and the above procedure is repeated to obtain the second spatial mode (EOT2), shown in Figure 2.1.7b. Smith (2004) calculated six rainfall modes in this way, though we will focus mainly on the first two modes, which together account for more than 80% of the variance. The third mode (Figure 2.1.7c) accounts for only 5% of the variance.

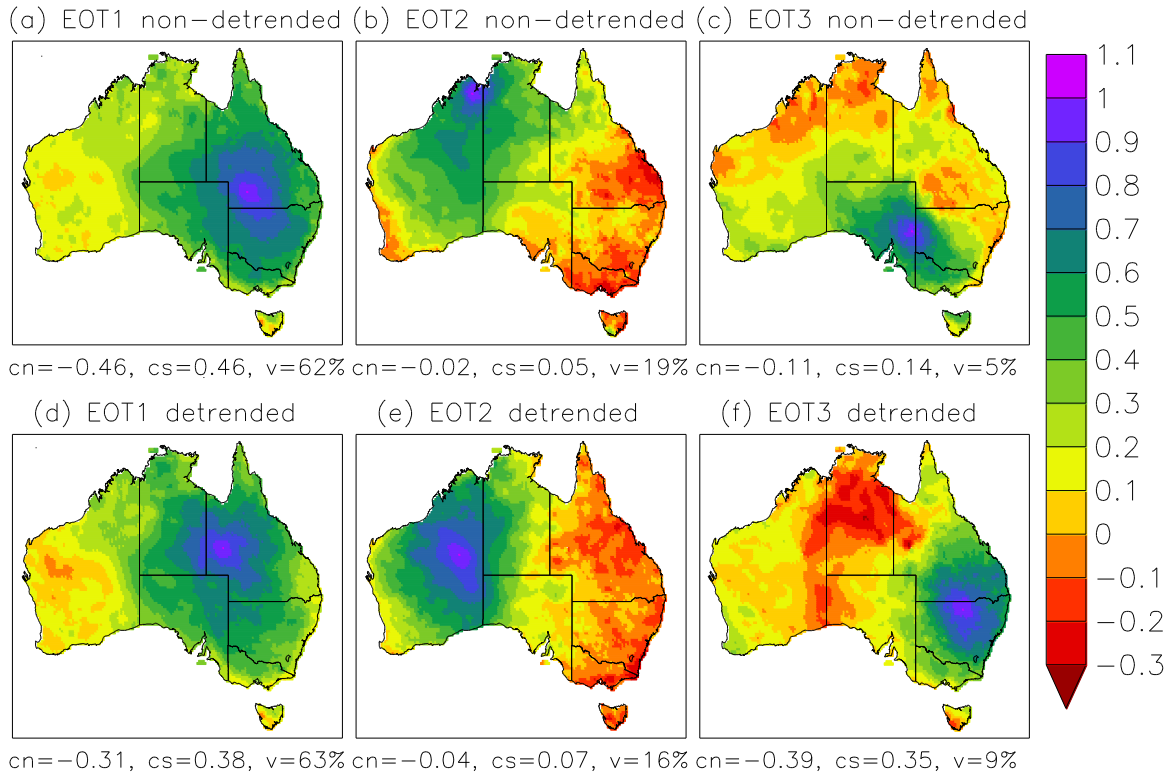


**Figure 2.1.7: First three modes (EOTs) of Australian annual rainfall variability, based on observations for the period 1901-2007. Upper panels (a-c) use raw (non-detrended) data; lower panels (d-f) use linearly detrended data. Below each panel, the correlation of the corresponding time series with annual Niño-3.4 region SST (*cn*) and the SOI (*cs*) are shown, as well as the percentage of variance (*v*) explained by that mode.**

Since we wish to compare observations with the results of the Mk3.6 simulation, which is an unforced model run, the data should preferably be detrended before performing the EOT analysis. The EOTs obtained using linearly detrended observations are shown in the lower panels of Figure 2.1.7. It is useful to compare the results obtained using raw and detrended data because it shows that there is some sensitivity to the details of the procedure. For example, using detrended data, the centre of the first mode is shifted to the north-west, relative to its location when raw data are used (Figures 2.1.7a and 2.1.7d). The correlation with Niño 3.4 SST and the SOI is weaker when detrended data are used, although the percentage of variance explained is similar. Interestingly, the detrended data generate a third mode that is offset to the south-east relative to the first mode, and also has the character of an ENSO-like mode (Figure 2.1.7f). The third mode actually has a stronger correlation with Niño 3.4 SST and the SOI than the first mode. A possible interpretation is that

the single ENSO-like mode obtained with raw data (Figure 2.1.7a) splits into two distinct modes when detrended data are used, each mode being offset in roughly opposite directions from the location of the original mode. In the comparison of observed and modelled EOTs below, we will focus on the first two modes; the third mode was included in Figure 2.1.7 mainly to show that, in the detrended observations, it takes the form of a second “ENSO-like” mode.

The second spatial mode (northwest or central-northwest mode) also looks somewhat different, depending on whether the data are detrended or not (Figures 2.1.7b and 2.1.7e). It is interesting that, even when the linear trend is removed, this appears as the second EOT, because it resembles the observed pattern of rainfall increase over northwest and central Australia in recent decades (Rotstayn *et al.*, 2007). This suggests that the observed rainfall increase over the northwest could reflect a natural mode of Australian rainfall variability that has received little attention (though it was discussed by Smith, 2004). It is also intriguing that the second mode resembles an east-west “flip-flop”, where wetter conditions in the northwest are associated with drier conditions in the east. If the northwest rainfall increase has indeed been driven by anthropogenic forcing (such as the Asian aerosol haze, as hypothesised by Rotstayn *et al.*, 2007) then this forcing may have also contributed to the drying trend in the east. Figure 8 shows the times series T1, T2 and T3 corresponding to the first three EOTs calculated from the non-detrended rainfall observations. It is seen that the time series showing the strongest trend in recent decades is indeed T2, corresponding to EOT2 (Figure 2.1.7b). The associated trend correlation coefficient ( $r = 0.33$ ) is significant over the period 1901 – 2007, despite the relatively low degrees of freedom (54). Using data for 1901 – 2002, Smith (2004) came to a similar conclusion, though he cautioned that rainfall stations are relatively sparse over the region where EOT2 is centred. Trends in T1 and T3 are not significant.

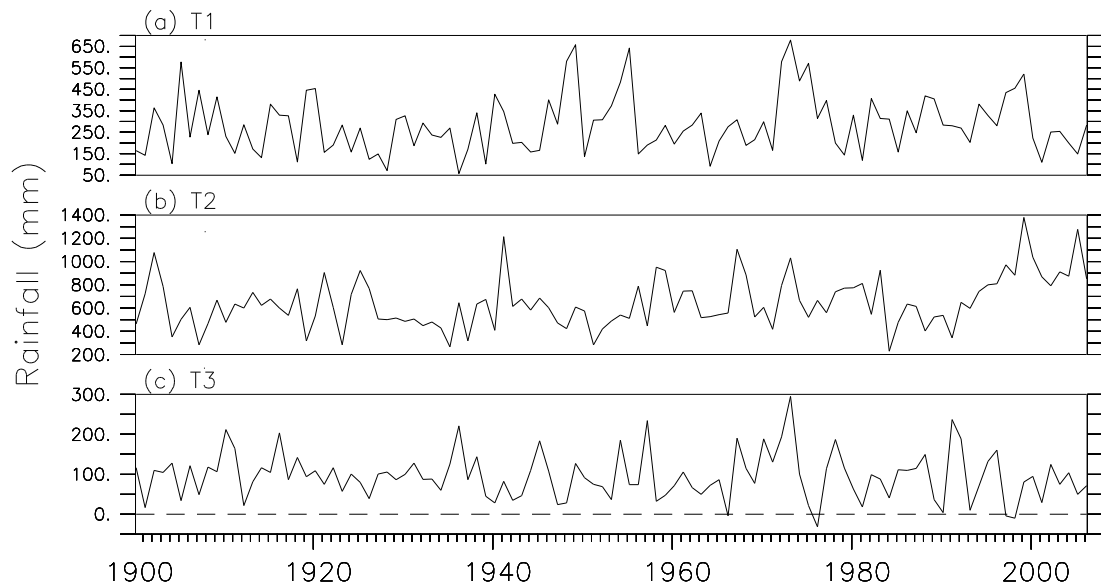


**Figure 2.1.8: Time series corresponding to the (non-detrended) observed rainfall EOTs shown in Figures 7(a), 7(b) and 7(c) respectively.**

Figure 2.1.9 shows the first EOT of annual Australian rainfall from the eight models referred to above. The Mk3.6 results are based on the 70-year coupled control run described above, and the other results are based on coupled model output for the period 1901 – 2000; all data were linearly detrended before applying the EOT analysis. Comparison of Figure 2.1.9 with Figures 2.1.7a and 2.1.7d suggests that CSIRO Mk3.6 is the model best able to capture the properties of the first rainfall EOT. Compared to the first EOT from the raw observations, the agreement is exceptionally good, both in terms of the spatial pattern, the correlations with Niño 3.4 SST and the SOI, and the explained variance. The agreement with the detrended observations is also good, although the correlations with Niño 3.4 SST ( $r = -0.47$ ) and the SOI ( $r = 0.50$ ) are stronger in the model than in the observations ( $r = -0.31$  and  $0.38$  respectively). For most of the models, the first rainfall mode shows a strong correlation with Niño 3.4 SST, in the range of  $-0.45$  to  $-0.68$ ; the exception is HadGEM1, which has a correlation of  $-0.21$ . In most models, the first rainfall mode also shows a strong correlation with the SOI, except for MRI ( $r = 0.09$ ) and, to a lesser extent, HadGEM1 ( $r = 0.24$ ). The explained variance ranges from 52% (HadGEM1) to 81% (Mk3.5 and GFDL). It is also noteworthy that HadGEM1 has the lowest regression coefficients for the first EOT, when averaged over the continent,

and that the pattern from MRI is less well defined than that from the other models. These results suggest that HadGEM1 and MRI have a “weak” ENSO teleconnection to Australia. HadGEM1 was one of several models identified by van Oldenborgh *et al.* (2005) as having weak ENSO-related SST variability in the equatorial Pacific, which may explain this result; we shall return to this point below. The only other model besides Mk3.6 that has the centre of the leading rainfall mode located over eastern Australia is ECHAM5, which was the model ranked highest for simulation of Australian mean climate by Suppiah *et al.* (2007).

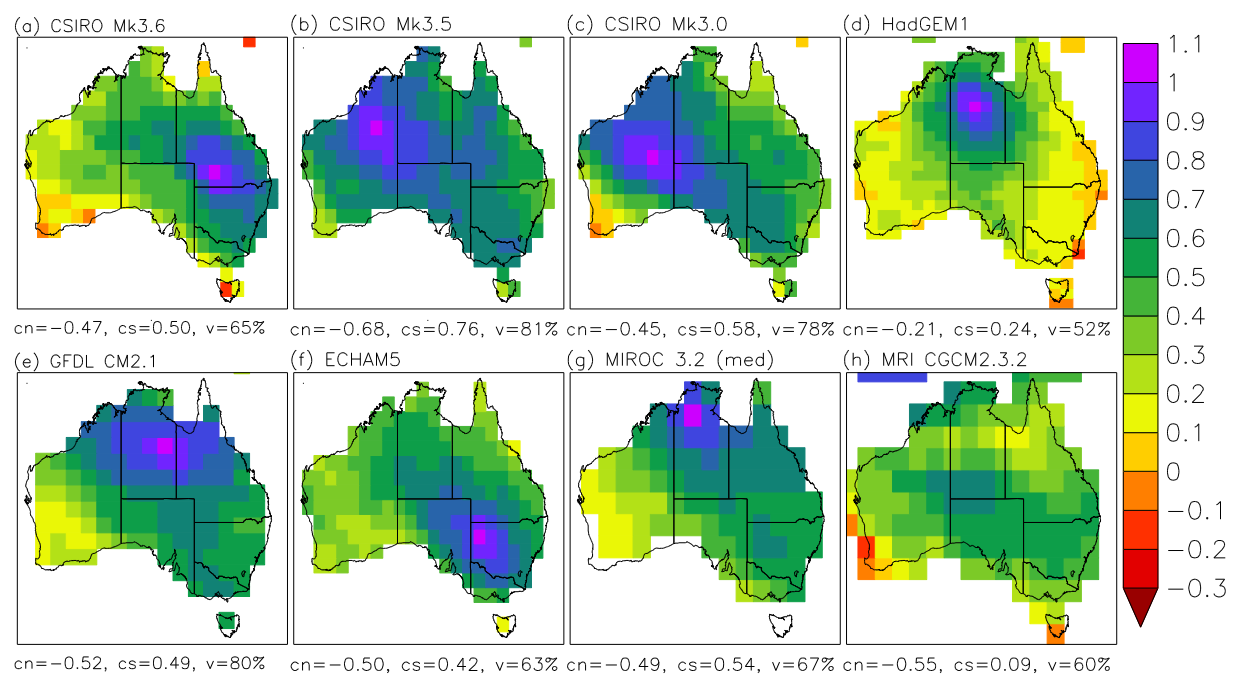


**Figure 2.1.9: First EOT of annual rainfall from (a) the CSIRO Mk3.6 GCM, and seven AR4 GCMs: (b) CSIRO Mk3.5 (c) CSIRO Mk3.0, (d) HadGEM1, (e) GFDL CM2.1, (f) ECHAM5, (g) MIROC 3.2 medium-resolution, (h) MRI CGCM2.3.2. Below each panel, the correlation of the corresponding time series with annual Niño-3.4 region SST (*cn*) and the SOI (*cs*) are shown, as well as the percentage of variance (*v*) explained by that mode.**

The second EOT of annual rainfall from each of the models is shown in Figure 2.1.10. As was the case for the first EOT, only Mk3.6 and ECHAM5 show any ability to capture the spatial pattern of the second observed rainfall EOT (Figures 2.1.7b and 2.1.7e). Mk3.6 is better at picking up the east-west “flip-flop” as suggested by the

observations. However, the second EOT in both models is too strongly correlated with Niño 3.4 SST and the SOI. This may be related to the excessive westward extension of the SST anomalies associated with ENSO in the models; see the comments below.

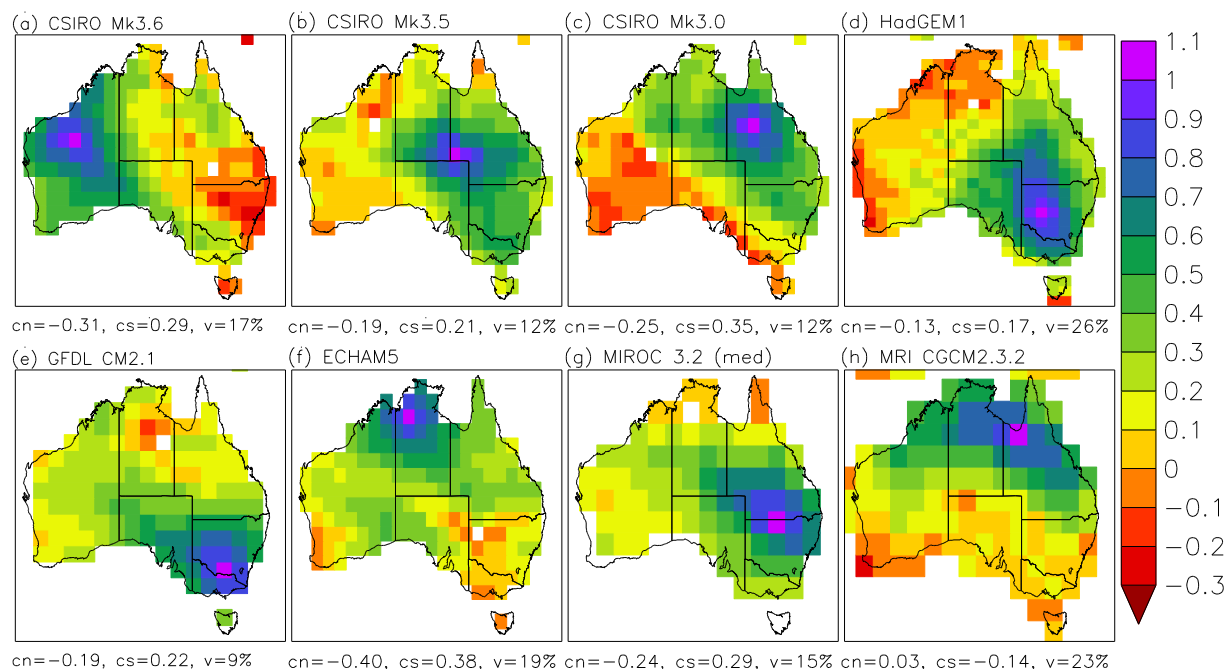


**Figure 2.1.10: As Figure 9, but for the second EOT.**

The spatial pattern and amplitude of SST variability associated with ENSO are both likely to affect the variability of Australian rainfall (Wang and Hendon, 2007; Shi *et al.*, 2008b, Cai *et al.*, 2009). Figure 2.1.11 shows the spatial pattern of one standard deviation of observed and modelled annual-mean SST anomalies associated with variability in the Niño 3.4 region. The first point is that all the models shown suffer from the usual equatorial Pacific “cold tongue” bias (Davey *et al.*, 2002; Sun *et al.*, 2006), which is manifested here as an excessive westward extension of the warm SST anomalies that are in phase with those in the Niño 3.4 region. This westward extension of the ENSO SST anomaly pattern causes the models to have an ENSO teleconnection pattern over Australia that also lies too far to the west (Shi *et al.*, 2008b; Cai *et al.*, 2009). In the previous section, most of the models had the leading rainfall mode centred too far west. Two models (Mk3.6 and ECHAM5) had the leading rainfall mode centred over eastern Australia, in reasonable agreement with observations. However, in both of these models, the second rainfall mode was too strongly correlated with ENSO.

Considering the amplitude of the SST variability, there are large differences among the models. Three models (GFDL, Mk3.5 and ECHAM5) have excessive SST variability in the equatorial Pacific region, shown by visual inspection of the plots and by the standard deviation of annual Niño 3.4 SST (in the legend of each panel). Mk3.0 (not shown) has a similar pattern to Mk3.5, but with a more realistic amplitude in the Niño 3.4 region (standard deviation = 0.62 °C). Four other models (Mk3.6, HadGEM1, MIROC and MRI) have Niño 3.4 SST variability that is slightly weaker than the observations, with Mk3.6 having the closest standard deviation to the observed (0.49 compared to 0.54 °C). In a survey of 24 AR4 models, Cai *et al.* (2009) found that the amplitude of Niño 3.4 SST variability exerted a systematic control on the ENSO-rainfall teleconnection to Australia, as measured by the correlation of grid-point rainfall with Niño 3.4 SST. As the ENSO amplitude increased from model to model, the ENSO-rainfall teleconnection generally strengthened, highlighting the importance of realistically simulating this attribute. Our EOT analysis also tends to support this argument: the two models with the largest ENSO amplitude (GFDL and Mk3.5) have the strongest ENSO rainfall teleconnections, with the largest explained variance for EOT1, strongest correlations of EOT1 with Niño 3.4 SST and the SOI, and largest regression

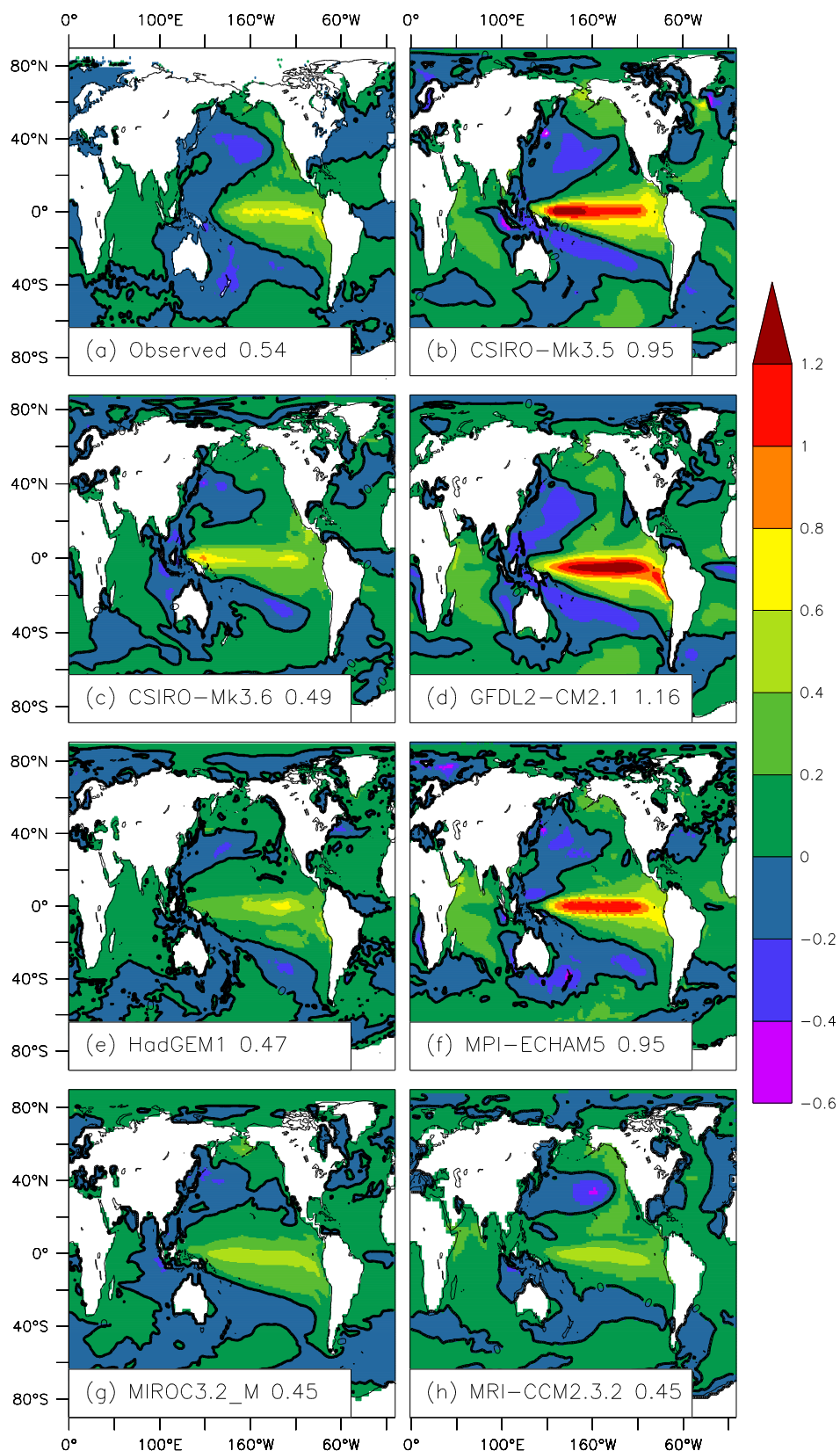


**Figure 2.1.11: Spatial pattern of one standard deviation of (a) observed and (b-h) modelled annual-mean SST anomalies associated with ENSO. The anomalies were constructed by multiplying regression coefficients (obtained by regressing**

**grid-point SST anomalies against the time series of Niño-3.4 SST) by one standard deviation of Niño-3.4 SST. The standard deviation of annual Niño-3.4 SST (°C) is shown in the legend of each panel.**

**Coefficients for EOT1 when averaged over the continent. Conversely, the models we identified as having “weak” ENSO teleconnections (HadGEM1 and MRI) are among those with the smallest ENSO amplitude. Aside from the ENSO amplitude, the spatial pattern is also likely to explain some of the inter-model differences, e.g., positive SST anomalies near the date line have been shown to have a larger effect on Australian rainfall than anomalies located further east (Wang and Hendon, 2007).**

#### *Summary and implications for Western Australia*

We assessed the simulation of Australian mean climate and rainfall variability in a new version of the CSIRO GCM. The new version (Mk3.6) differs from its recent predecessors (Mk3.0 and Mk3.5) in that it includes a comprehensive, interactive aerosol scheme. Comparison of the mean summer and winter climate simulations in Mk3.6 with those in Mk3.0 and Mk3.5 showed several encouraging improvements in the new version, especially regarding winter rainfall and MSLP. The impression of an overall improvement in the model’s simulation of Australian mean climate was confirmed by calculation of a non-dimensional skill score *M* (Watterson, 1996; Meehl *et al.*, 2007), based on data from all four seasons. The improved value of *M* obtained for Mk3.6 would rank it fifth out of 24 GCMs, if it were included in Table 2.1.1 of Watterson (2008). Mk3.5 and Mk3.0 were respectively ranked 12<sup>th</sup> and equal 13<sup>th</sup> of 23 AR4 GCMs by Watterson (2008). The improved simulation of winter rainfall over south-western WA makes the Mk3.6 model potentially attractive for use in downscaling studies over that region.

The most dramatic improvement in Mk3.6 was in the model’s simulation of the leading modes of annual rainfall variability. Mk3.6 was best able to capture the spatial pattern of the leading “ENSO-related” rainfall mode, which is centred over eastern Australia, whereas the earlier versions incorrectly located the centre of this mode over WA. This improvement is important, because if the ENSO-related mode in the model is located over northern WA, the simulated rainfall response there may be unrealistically dominated by the response of ENSO to the applied forcing.

The analysis was repeated using output from several other AR4 GCMs, including three that were recently assessed as providing good simulations of Australian mean seasonal climate (Suppiah *et al.*, 2007; Watterson, 2008). Of the models considered, Mk3.6 had the best simulation of the spatial pattern of the two leading modes of Australian rainfall variability. The second rainfall mode, centred over north-western WA, was also captured best by Mk3.6, although the correlation of this mode with ENSO was too strong. This is probably related to an excessive westward extension of the ENSO-related sea-surface temperature anomalies, a typical GCM bias that was seen in all the models. The simulation of the amplitude of ENSO-related SST variability in Mk3.6 also compared favourably with other models we considered; this may have also contributed to its improved simulation of Australian rainfall variability.

An accurate simulation of the first rainfall mode is important for studies of Australian climate change, because this mode correlates strongly with ENSO, which dominates rainfall variability over most of eastern and central Australia. The second rainfall mode is also potentially important, because its observed time series shows a significant upward trend in recent decades, corresponding to increased rainfall over northern WA, and decreased rainfall over eastern Australia. With regard to the aims of this project, it is encouraging that the Mk3.6 GCM is able to capture this pattern as an unforced mode of natural variability (though its physical meaning is currently unexplained). It will be most interesting to see whether this mode responds differently in time-varying simulations that include changes in Asian aerosol forcing, as hypothesized by Rotstayn (2007).

## **References**

- Allan, R. J., and T. J. Ansell, 2006. A new globally complete monthly historical mean sea level pressure data set (HadSLP2): 1850 – 2004, *J. Clim.*, 19, 5816– 5842.
- Arblaster, J. M., and G. A. Meehl, 2006. Contributions of external forcings to Southern Annular Mode trends, *J. Clim.*, 19, 2896–2905.
- Ashok, K., Z. Guan, and T. Yamagata, 2003. Influence of the Indian Ocean Dipole on the Australian winter rainfall, *Geophys. Res. Lett.*, 30(15), 1821, doi:10.1029/2003GL017926.

- Cai W, Bi D, Church J, Cowan T, Dix MR, Rotstayn LD. 2006. Panoceanic response to increasing anthropogenic aerosols: impacts on the Southern Hemisphere oceanic circulation. *Geophysical Research Letters* **33**: L21707, DOI:10.1029/2006GL027513.
- Cai, W., M. A. Collier, H. B. Gordon, and L. J. Waterman, 2003a. Strong ENSO variability and a Super-ENSO pair in the CSIRO Mark 3 coupled climate model, *Mon. Weather Rev.*, 31, 1189–1210.
- Cai W., T. Cowan, 2007. Impacts of increasing anthropogenic aerosols on the atmospheric circulation trends of the Southern Hemisphere: An air-sea positive feedback, *Geophys. Res. Lett.*, 34, L23709, doi:10.1029/2007GL031706.
- Cai W, Cowan T, Dix MR, Rotstayn LD, Ribbe J, Shi G, Wijffels S. 2007. Anthropogenic aerosol forcing and the structure of temperature trends in the Southern Indian Ocean. *Geophysical Research Letters* **34**: L14611, DOI:10.1029/2007GL030380.
- Cai, W., G. Shi, and Y. Li, 2005. Multidecadal fluctuations of winter rainfall over southwest Western Australia simulated in the CSIRO Mark 3 coupled model, *Geophys. Res. Lett.*, 32, L12701, doi:10.1029/2005GL022712.
- Cai, W., A. Sullivan and T. Cowan, 2009. Rainfall teleconnections with Indo-Pacific variability in the IPCC AR4 models. *J. Climate*, in press, DOI: 10.1175/2009JCLI2694.1.
- Cai, W., P. H. Whetton, and D. J. Karoly, 2003b. The response of the Antarctic oscillation to increasing and stabilized atmospheric CO<sub>2</sub>, *J. Clim.*, 16, 1525–1538.
- Davey, M., M. Huddleston, K. Sperber, P. Braconnot, F. Bryan, D. Chen, R. Colman, C. Cooper, U. Cubasch, P. Delecluse, D. DeWitt, L. Fairhead, G. Flato, C. Gordon, T. Hogan, M. Ji, M. Kimoto, A. Kitoh, T. Knutson, M. Latif, H. Le Treut, T. Li, S. Manabe, C. Mechoso, G. Meehl, S. Power, E. Roeckner, L. Terray, A. Vintzileos, R. Voss, B. Wang, W. Washington, I. Yoshikawa, J. Yu, S. Yukimoto, S. Zebiak, 2002. STOIC: A study of coupled model climatology and variability in tropical ocean regions. *Climate Dyn.*, **18**, 403–420.
- Flannery, T.F., 2007. If scientists' hands are tied, we fly partly blind into the future. *The Age*, 29 January 2007. Available at

<http://www.theage.com.au/news/opinion/we-fly-partly-blind-into-the-future/2007/01/28/1169919208494.html?page=fullpage#contentSwap1>.

- Gordon, H.B., Rotstayn, L.D., McGregor, J.L., Dix, M.R., Kowalczyk, E.A., O'Farrell, S.P., Waterman, L.J., Hirst, A.C., Wilson, S.G., Collier, M.A., Watterson, I.G. and Elliott, T.I.
2002. The CSIRO Mk3 Climate System Model, *CSIRO Atmospheric Research Technical Paper No. 60.*, 134 pp. Available online at [http://www.cmar.csiro.au/e-print/open/gordon\\_2002a.pdf](http://www.cmar.csiro.au/e-print/open/gordon_2002a.pdf).
- Jones, D.A., Weymouth, G.T. 1997. *An Australian monthly rainfall dataset*. Technical Report 70, Bureau of Meteorology, Melbourne, Australia, 19 pp.
- Jones, D.A., Trewin, B.C. 2000. The spatial structure of monthly temperature anomalies over Australia. *Australian Meteorological Magazine*, **49**, 261-276.
- McBride, J.L. and N. Nicholls, 1983. Seasonal relationships between Australian rainfall and the Southern Oscillation. *Mon. Wea. Rev.*, 111, 1998-2004.
- Meehl, G.A., T.F. Stocker, W.D. Collins, P. Friedlingstein, A.T. Gaye, J.M. Gregory, A. Kitoh, R. Knutti, J.M. Murphy, A. Noda, S.C.B. Raper, I.G. Watterson, A.J. Weaver and Z.-C. Zhao, 2007: Global Climate Projections. In: *Climate Change 2007: The Physical Science Basis. Contribution of Working Group I to the Fourth Assessment Report of the Intergovernmental Panel on Climate Change* [Solomon, S., D. Qin, M. Manning, Z. Chen, M. Marquis, K.B. Averyt, M. Tignor and H.L. Miller (eds.)]. Cambridge University Press, Cambridge, United Kingdom and New York, NY, USA.
- Meneghini, B., I. Simmonds, and I. N. Smith, 2007. Association between Australian rainfall and the Southern Annular Mode, *Int. J. Climatol.*, **27**, 109-121, doi:10.1002/joc.1370.
- Mohalfi, S., H.S. Bedi, T.N. Krishnamurti, and S.D. Cocke, 1998. Impact of Shortwave Radiative Effects of Dust Aerosols on the Summer Season Heat Low over Saudi Arabia. *Mon. Wea. Rev.*, **126**, 3153–3168.
- Pitman, A. J., G. T. Narisma, R. A. Pielke, and N. J. Holbrook, 2004. Impact of land cover change on the climate of southwest Western Australia, *J. Geophys. Res.*, **109**, D18109, doi: 10.1029/2003JD004347.
- Rayner, N. A., D. E. Parker, E. B. Horton, C. K. Folland, L. V. Alexander, D. P. Rowell, E. C. Kent, and A. Kaplan, 2003. Globally complete analyses of sea

- surface temperature, sea ice and night marine air temperature, *J. Geophys. Res.*, **108**(D14), 4407, doi:10.1029/2002JD002670.
- Ropelewski, C. F., and M. S. Halpert, 1987. Global and regional scale precipitation associated with El Niño/Southern Oscillation, *Mon. Weather Rev.*, 115, 1606–1626.
- Rotstayn, LD, 1997. A physically based scheme for the treatment of stratiform clouds and precipitation in large-scale models. I: Description and evaluation of the microphysical processes. *Quart. J. Roy. Meteor. Soc.*, **123**, 1227–1282.
- Rotstayn, LD, 1998. A physically based scheme for the treatment of stratiform clouds and precipitation in large-scale models. II: Comparison of modelled and observed climatological fields. *Quart. J. Roy. Meteor. Soc.*, **124**, 389–415.
- Rotstayn, LD, 1999. Climate Sensitivity of the CSIRO GCM: Effect of Cloud Modeling Assumptions. *J. Climate*, **12**, 334–356.
- Rotstayn LD, Cai W, Dix MR, Farquhar GD, Feng Y, Ginoux P, Herzog M, Ito A, Penner JE, Roderick ML, Wang M. 2007. Have Australian rainfall and cloudiness increased due to the remote effects of Asian anthropogenic aerosols? *Journal of Geophysical Research* **112**: D09202, DOI:10.1029/2006JD007712.
- Rotstayn, L. D., M. A. Collier, M. R. Dix, Y. Feng, H. B. Gordon, S. P. O'Farrell, I. N. Smith, J. Syktus, 2009: Improved simulation of Australian climate and ENSO-related rainfall variability in a GCM with an interactive aerosol treatment. *Int. J. Climatol.*, in press, DOI: 10.1002/joc.1952.
- Rotstayn, LD, Keywood, MD, Forgan, BW, Gabric, AJ, Galbally, IE, Gras, JL, Luhar, AK, McTainsh, GH, Mitchell, RM, Young, SA, 2008. Possible impacts of anthropogenic and natural aerosols on Australian climate: a review. *International Journal of Climatology*, DOI: 10.1002/joc.1729.
- Rotstayn LD, Liu Y. 2003. Sensitivity of the first indirect aerosol effect to an increase of cloud droplet spectral dispersion with droplet number concentration. *Journal of Climate* **16**: 3476–3481.
- Rotstayn LD, Liu Y. 2005. A smaller global estimate of the second indirect aerosol effect. *Geophysical Research Letters* **32**: L05708, DOI:10.1029/2004GL021922.
- Rotstayn LD, Lohmann U. 2002a. Tropical rainfall trends and the indirect aerosol effect. *Journal of Climate* **15**: 2103–2116.

- Rotstayn LD, Lohmann U. 2002b. Simulation of the tropospheric sulfur cycle in a global model with a physically based cloud scheme. *Journal of Geophysical Research* **107**: 4592, DOI: 10.1029/2002JD002128.
- Saji, N. H., B. N. Goswami, P. N. Vinayachandran, and T. Yamagata, 1999. A dipole mode in the tropical Indian Ocean, *Nature*, 401, 360–363.
- Shi, G., W. Cai, T. Cowan, J. Ribbe, L.D. Rotstayn, and M.R. Dix, 2008a. Variability and trend of the northwest Western Australia Rainfall: observations and coupled climate modeling. *J. Climate*, **21**, 2938–2959, DOI: 10.1175/2007JCLI1908.1.
- Shi G., J. Ribbe, W. Cai, T. Cowan, 2008b. An interpretation of Australian rainfall projections, *Geophys. Res. Lett.*, 35, L02702, doi:10.1029/2007GL032436.
- Smith IN, 2004. An assessment of recent trends in Australian rainfall. *Australian Meteorological Magazine* **53**, 163-173.
- Smith IN, 2007. Global climate modelling within CSIRO: 1981 to 2006. *Aust. Meteorol. Mag.* **56**: 153-166.
- Sun, D.Z., T. Zhang, C. Covey, S.A. Klein, W.D. Collins, J.J. Hack, J.T. Kiehl, G.A. Meehl, I.M. Held, and M. Suarez, 2006. Radiative and Dynamical Feedbacks over the Equatorial Cold Tongue: Results from Nine Atmospheric GCMs. *J. Climate*, **19**, 4059–4074.
- Suppiah, R., Hennessy, K.J., Whetton, P.H., McInnes, K., Macadam, I, Bathols, J., Ricketts, J. and Page, C.M. 2007. Australian climate change projections derived from simulations performed for the IPCC 4th Assessment Report. *Aust. Meteorol. Mag.*, 56, 131-52.
- Takemura, T., H. Okamoto, Y. Maruyama, A. Numaguti, A. Higurashi, and T. Nakajima, 2000. Global three-dimensional simulation of aerosol optical thickness distribution of various origins, *J. Geophys. Res.*, 105(D14), 17,853–17,873.
- Timbal B, JM Arblaster, 2006. Land cover change as an additional forcing to explain the rainfall decline in the south west of Australia, *Geophys. Res. Lett.*, 34, L07717, doi:10.1029/2005GL025361
- Timbal, B., J. M. Arblaster, and S. Power, 2006. Attribution of the late-twentieth-century rainfall decline in Southwest Australia, *J. Clim.*, 19, 2046– 2062.
- Van den Dool, HM, Saha, S, Johansson, A, 2000. Empirical orthogonal teleconnections. *Journal of Climate* **13**, 1421-1435.

- van Oldenborgh GJ, Philip SY, Collins M, 2005. El Niño in a changing climate: a multi-model study. *Ocean Sci* 1:81–95.
- Wang, G., and H. H. Hendon, 2007. Sensitivity of Australian Rainfall to Inter–El Niño Variations. *J. Climate*, 20, 4211–4226.
- Watterson, I. G., 1996. Non-dimensional measures of climate model performance, *Int. J. Climatol.*, 16, 379–391.
- Watterson I. G., 2008. Calculation of probability density functions for temperature and precipitation change under global warming, *J. Geophys. Res.*, **113**, D12106, doi:10.1029/2007JD009254.

### LIST OF TABLES

Table 2.1.1:	AR4 models used in this study, with their ranking (out of 23 models) for simulation of Australian mean seasonal climate from Suppiah et al. (2007) and Watterson (2008). .....	9
Table 2.2.2:	Model – observed pattern correlations and RMS errors (°C) for surface air temperature over Australia.....	12
Table 2.1.3:	Model – observed pattern correlations and RMS errors (hPa) for MSLP over Australia .....	14
Table 2.1.4:	Model – observed pattern correlations and RMS errors (mm/day) for precipitation over Australia.....	16

### LIST OF FIGURES

Figure 2.1.1:	JJA surface air temperature in °C, (a) from observations for the period 1981-1999, and simulated by three versions of the CSIRO GCM: (b) Mk3.0, (c) Mk3.5 and (d) Mk3.6.	13
Figure 2.1.2:	DJF surface air temperature in °C, (a) from observations for the period 1981-1999, and simulated by three versions of the CSIRO GCM: (b) Mk3.0, (c) Mk3.5 and (d) Mk3.6.	14
Figure 2.1.3:	JJA mean sea-level pressure in hPa, (a) from observations for the period 1981-1999, and simulated by three versions of the CSIRO GCM: (b) Mk3.0, (c) Mk3.5 and (d) Mk3.6.	15
Figure 2.1.4:	DJF mean sea-level pressure in hPa, (a) from observations for the period 1981-1999, and simulated by three versions of the CSIRO GCM: (b) Mk3.0, (c) Mk3.5 and (d) Mk3.6.	16
Figure 2.1.5:	JJA precipitation in mm/day, (a) from observations for the period 1981-1999, and simulated by three versions of the CSIRO GCM: (b) Mk3.0, (c) Mk3.5 and (d) Mk3.6.	17

- Figure 2.1.6: DJF precipitation in mm/day, (a) from observations for the period 1981-1999, and simulated by three versions of the CSIRO GCM: (b) Mk3.0, (c) Mk3.5 and (d) Mk3.6. 17
- Figure 2.1.7: First three modes (EOTs) of Australian annual rainfall variability, based on observations for the period 1901-2007. Upper panels (a-c) use raw (non-detrended) data; lower panels (d-f) use linearly detrended data. Below each panel, the correlation of the corresponding time series with annual Niño-3.4 region SST (cn) and the SOI (cs) are shown, as well as the percentage of variance (v) explained by that mode. 20
- Figure 2.1.8: Time series corresponding to the (non-detrended) observed rainfall EOTs shown in Figures 7(a), 7(b) and 7(c) respectively. 22
- Figure 2.1.9: First EOT of annual rainfall from (a) the CSIRO Mk3.6 GCM, and seven AR4 GCMs: (b) CSIRO Mk3.5 (c) CSIRO Mk3.0, (d) HadGEM1, (e) GFDL CM2.1, (f) ECHAM5, (g) MIROC 3.2 medium-resolution, (h) MRI CGCM2.3.2. Below each panel, the correlation of the corresponding time series with annual Niño-3.4 region SST (cn) and the SOI (cs) are shown, as well as the percentage of variance (v) explained by that mode. 23
- Figure 2.1.10: As Figure 9, but for the second EOT. 24
- Figure 2.1.11: Spatial pattern of one standard deviation of (a) observed and (b-h) modelled annual-mean SST anomalies associated with ENSO. The anomalies were constructed by multiplying regression coefficients (obtained by regressing grid-point SST anomalies against the time series of Niño-3.4 SST) by one standard deviation of Niño-3.4 SST. The standard deviation of annual Niño-3.4 SST (°C) is shown in the legend of each panel. 26